

Pyramidal Dense Attention Networks for Lightweight Image Super-Resolution

Huapeng Wu, Jie Gui, *Senior Member, IEEE*, Jun Zhang, *Member, IEEE*, James T. Kwok, *Fellow, IEEE*, and Zhihui Wei, *Member, IEEE*

Abstract—Recently, deep convolutional neural network methods have achieved an excellent performance in image super-resolution (SR), but they can not be easily applied to embedded devices due to large memory cost. To solve this problem, we propose a pyramidal dense attention network (PDAN) for lightweight image super-resolution in this paper. In our method, the proposed pyramidal dense learning can gradually increase the width of the densely connected layer inside a pyramidal dense block to extract deep features efficiently. Meanwhile, the adaptive group convolution that the number of groups grows linearly with dense convolutional layers is introduced to relieve the parameter explosion. Besides, we also present a novel joint attention to capture cross-dimension interaction between the spatial dimensions and channel dimension in an efficient way for providing rich discriminative feature representations. Extensive experimental results show that our method achieves superior performance in comparison with the state-of-the-art lightweight SR methods.

Index Terms—Super-resolution, pyramidal dense learning, group convolution, joint attention.

I. INTRODUCTION

Single image super-resolution (SISR) is a low-level vision problem that recovers a high resolution (HR) image from a low resolution (LR) observation, which is an ill-posed problem because multiple HR images can be degraded to the same LR image. To address this issue, researchers have proposed many approaches, which can be divided into three subclasses including interpolation-based methods [1], reconstruction-based methods [2], and learning-based methods [3–10].

Benefit from the powerful learning ability, various deep convolutional neural network based methods have been introduced and achieved a significant performance in image SR community [11]. Firstly, Dong et al. [4] proposed a three-layer super-resolution convolutional neural network (SRCNN)

to learn the nonlinear mapping function between LR and HR. Later, inspired by ResNet [12] and DenseNet [13], many complex deep neural networks [14, 15] have been presented to boost reconstruction performance. However, doing so will cause an increase in model parameters and computational cost, which greatly limit their practical applications in some computing devices, such as mobile and embedded applications. For solving these problems, some network architectures have been proposed by integrating recursive learning and lightweight models. For example, Deeply-Recursive Convolutional Network (DRCN) [5] and Deep Recursive Residual Network (DRRN) [6] used a recursive network to reduce the number of network parameters by parameter sharing strategies. Although DRCN and DRRN show favorable performances with a few parameters, they have a deeper model (DRRN ups to 52 convolutional layers) and require heavy computational costs. To further save computational overhead, some works proposed to directly extract feature in LR domain, and then upscale the features by deconvolution [16] or sub-pixel convolution [17] at the end of the network. Afterward, Enhanced Deep Super-Resolution network (EDSR) [8] adopted this post-processing strategy and employed a simplified ResNet architecture, which has about 165 convolutional layers. Zhang et al. [18] utilized residual-in-residual structure by adding channel attention block to construct a very deep model (up to 400 layers) for training a SR model. From these efforts, we find that the deeper network is helpful to extract more feature information to reconstruct HR images, but most of them suffered from large network parameters and computational cost.

Recently, some other researchers began to focus on design lightweight and efficient neural networks for image SR. Ahn et al. introduced a cascading residual network (CARN) [19] to achieve efficient SR by using several cascading connections with group convolution [20]. The information distillation network (IDN) [21] employed information distillation mechanism to divide the intermediate features into two parts, one part was retained and another part was further processed by succeeding convolution operations. To better balance performance and inference applications, Hui et al. [22] further proposed a lightweight information multi-distillation network (IMDN) that extracted hierarchical features at a granular level, and split the preceding extracted features along channel dimension. At each step, its partial feature information was retained and the other features were processed in a subsequent step. It won the first place in the AIM 2019 constrained image super-resolution challenge [23]. In addition to the above-mentioned strategies, some other efficient methods (e.g. MobileNet [24], self-

This work was supported in part by the National Natural Science Foundation of China under Grant 11431015, Grant 61671243, Grant 61971223, Grant 61572463 and the Fundamental Research Funds for the Central Universities. Corresponding author: Zhihui Wei (e-mail: gswei@njust.edu.cn).

Huapeng Wu is with the School of Computer Science and Engineering, Nanjing University of Science and Technology, 210094, China.

Jie Gui is with the School of Cyber Science and Engineering, Southeast University, 211100, China.

Jun Zhang is with the School of Science, Nanjing University of Science and Technology, 210094, China.

James T. Kwok is with the Department of Computer Science and Engineering, Hong Kong University of Science and Technology, Hong Kong.

Zhihui Wei (corresponding author: gswei@njust.edu.cn) is with the School of Computer Science and Engineering, Nanjing University of Science and Technology, 210094, China, and with the School of Science, Nanjing University of Science and Technology, 210094, China.

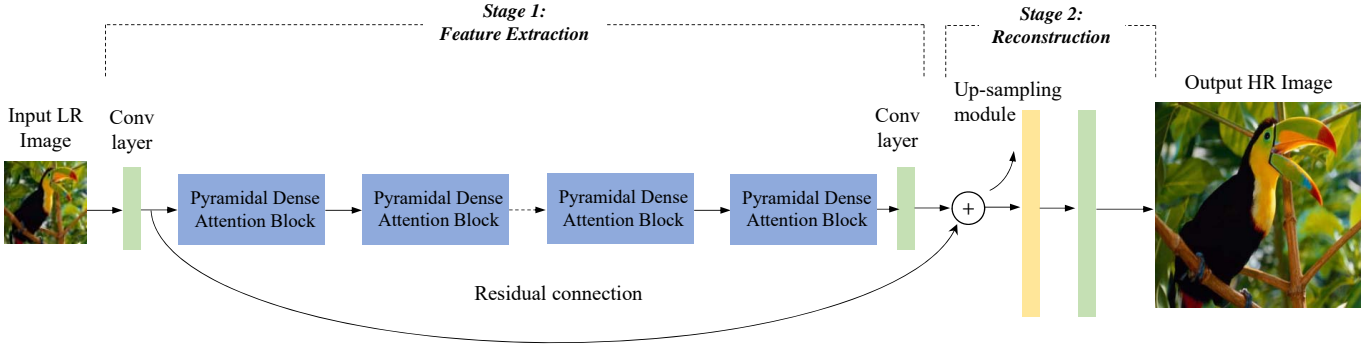


Fig. 1. The architecture of our pyramidal dense attention network (PDAN).

calibrated convolution [25] and network architecture search [26]) have also been proposed to design a lightweight deep neural network. Although these methods obtained comparable results, there is still room to obtain a better trade-off between model lightweight and SR performance.

In recent years, attention mechanisms have been widely used in many computer vision tasks and achieved good results [18, 27]. Hu et al. [28] proposed the squeeze-and-excitation block to learn the channel-wise information and improve the representation ability of the model. Inspired by [28], Zhang et al. [18] introduced a residual channel attention network (RCAN) by integrating the squeeze-and-excitation block into the residual architecture for image SR. In [29], the channel attention and spatial attention are combined to adaptively capture rich contextual information. Although these attention-based networks have provided performance improvements, they have some shortcomings. For example, SENet [28] only concentrate on channel-wise attention and ignore the importance of spatial information. Its variant, [29] uses the channel and spatial attention mechanisms, but they are only computed independently, which is also not beneficial to capture rich discriminative feature representations.

In this paper, we propose a novel lightweight pyramidal dense attention network (PDAN) for SISR (illustrated in Fig. 1). Unlike most previous dense networks with a fixed channel growth rate, we introduce a lightweight pyramidal dense block with a various channel growth rate inspired by [30]. The proposed feature extractor adopts the pyramidal dense learning strategy that the output channel dimensionality grows up while the convolutional layers are deepening in each pyramidal dense block, which can effectively aggregate contextual information (shown in Fig. 2). While increasing the output feature dimensionality is beneficial to enhance the feature learning ability of the networks, the parameter explosion needs to be noted. Therefore, we use group convolution with the dimension cardinality (i.e. the number of groups in each convolutional layer) which increases linearly to relieve the parameter explosion. Besides, to further improve the discriminative representation ability of the network, we propose a novel joint attention to capture cross-dimension interaction between the channel dimension and the spatial dimensions [31] for high-frequency information extraction. The detail of joint attention is shown in Fig. 2 (b), where

an input tensor (the size is $C \times H \times W$) is transferred to four branches, two of which are responsible for modeling channel attention ($C \times 1 \times 1$) and spatial attention (H, W) respectively, and the other two branches are used to build cross-dimension interaction between the channel dimension C and the spatial dimension H or W .

The main contributions of this paper are summarized as follows:

- (1) We propose a lightweight pyramidal dense attention network (PDAN) for SISR. The proposed lightweight model can effectively improve SR performance via the pyramidal dense feature learning and joint attention mechanism with a few parameters.
- (2) We introduce a pyramidal dense block to fully exploit multi-level features as well as boost the flow of information with a few parameters. Moreover, the proposed joint attention can efficiently capture cross-dimension interaction between the channel dimension and the spatial dimensions to provide richer and more discriminative contextual information for feature rescaling. In comparison with state-of-the-art lightweight SR methods, our method achieves competitive results in terms of model size and performance.

The remainder of this paper is organized as follows. In Section II, we introduce the proposed PDAN for image SR in detail. Extensive experimental results and analysis are provided in Section III. Finally, the conclusion is given in Section IV.

II. PROPOSED METHOD

In this section, we will show the proposed lightweight pyramidal dense attention networks for SISR in details.

A. Network Architecture

As illustrated in Fig. 1, the proposed PDAN consists of two modules: 1) feature extraction module, 2) reconstruction module. In this paper, we denote I^{LR} and I^{SR} as the input LR image and output HR image of our PDAN. The LR image is first fed to one 3×3 convolution layer for initial feature extraction. Next, the learned initial features are fed into several stacked lightweight pyramidal dense attention blocks to produce powerful feature maps. Lastly, we apply the reconstruction module that consists of a 3×3 convolution

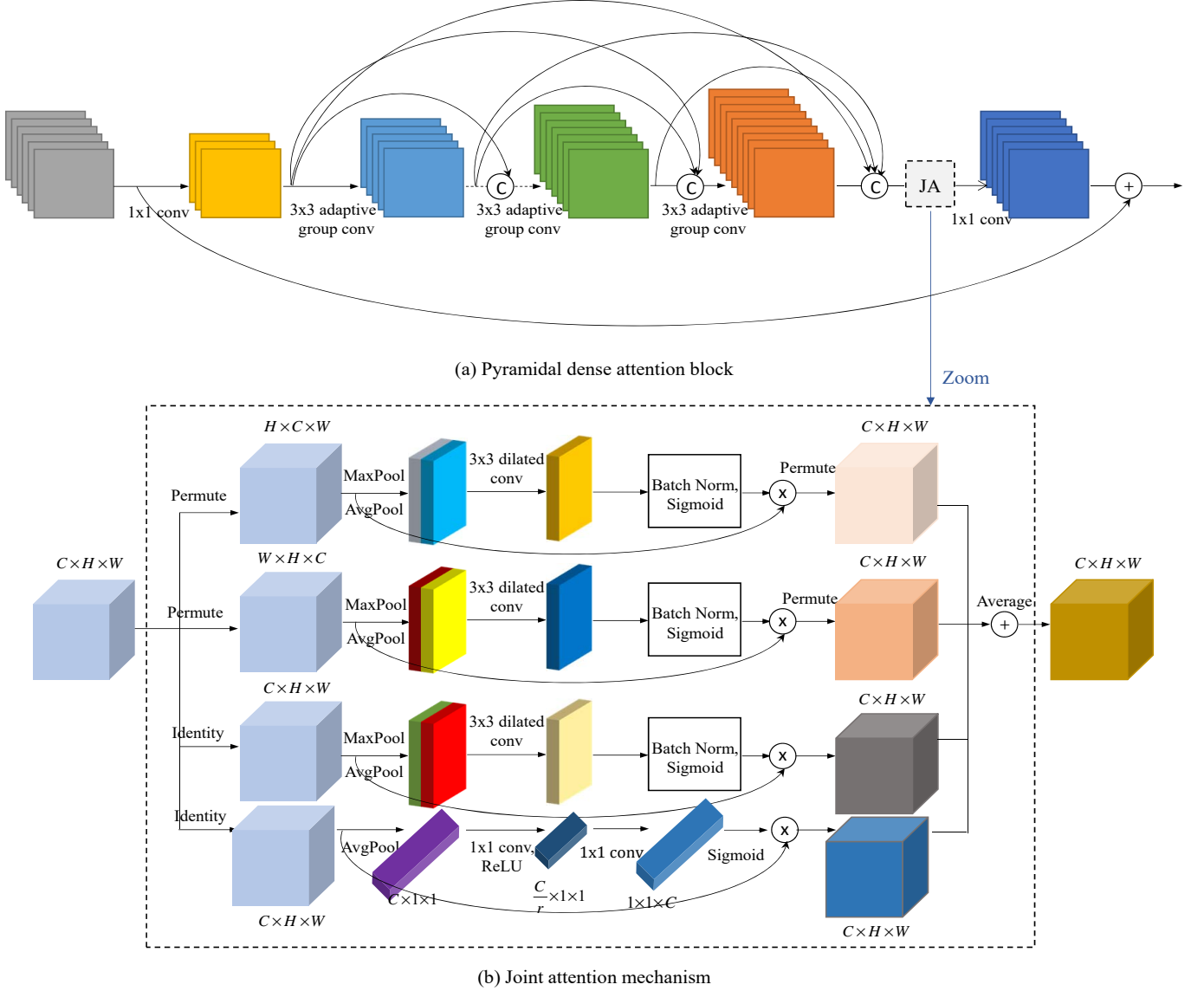


Fig. 2. (a) The illustration of the proposed pyramidal dense attention block. (b) The details of the joint attention module.

layer and a sub-pixel convolution layer [17] to reconstruct the desired SR image. The SR procedure of the proposed PDAN can be written as following:

$$I^{SR} = F_{PDAN}(I^{LR}, \theta) = F_{UP}(F_e(I^{LR})), \quad (1)$$

where F_{PDAN} represents the reconstruction function of our PDAN, θ denotes the learnable parameters of the network, F_e is the feature extraction step and F_{up} denotes the up-sampling and reconstruction step.

Our PDAN is optimized with the L_1 loss [18] by measuring the difference between a reconstructed SR image I^{SR} and its HR ground-truth I^{HR} . Given a set of training image pairs $\{I_i^{LR}, I_i^{HR}\}_{i=1}^N$, where N denotes the number of training images. The loss function of our method can be expressed as

$$L(\theta) = \frac{1}{N} \sum_{i=1}^N \|F_{PDAN}(I_i^{LR}, \theta) - I_i^{HR}\|_1. \quad (2)$$

Next, we will give more details about the proposed lightweight pyramidal dense attention block.

B. Pyramidal Dense Attention Block (PDAB)

As illustrated in Fig. 2 (a), our pyramidal dense attention block (PDAB) is mainly constructed by two stages: pyramidal dense feature learning, and feature refinement based on joint attention mechanism. Moreover, local residual learning is also adopted to improve the gradient information flow. Let H_{d-1} and H_d denote the input and output of the d -th PDAB, respectively. The process flow with PDAB can be formulated as following:

$$H_d = H_{d-1} + F_{PDAB}(H_{d-1}), \quad (3)$$

where F_{PDAB} is the mapping function of the proposed PDAB.

1) *Pyramidal Dense Feature Learning*: Dense skip connections have been widely exploited in deep learning methods, which is beneficial to boost the flow of feature information and

enhance the representation ability of the network. However, on the other hand, the dense connections will need large resources and memory for extracting and storing features. Additionally, due to the inconsistency between the number of input and output channels, the dense connections with a fixed channel growth rate can cause the loss of information and degrade the learning ability of the network. In this paper, we introduce a pyramidal dense connection mechanism with a varying growth rate, where the output feature dimensionality of convolutional layers gradually increases when the network layers are deepening to relieve this problem. However, when the convolution layers increase, this method will result in the parameter explosion. Specifically, the input channel dimensionality of two different dense connection layers can be written as follows.

The conventional dense connections with a fixed growth rate are

$$C_i = c_0 + \sum_{j=1}^{i-1} c_j = c_0 + (i-1) \times g_0, \quad (4)$$

$$c_j = g_0. \quad (5)$$

The pyramidal dense connections with a varying growth rate are

$$\tilde{C}_i = c_0 + \sum_{j=1}^{i-1} \tilde{c}_j = c_0 + (i-1) \times g_0 + g \times \frac{(i-1)(i-2)}{2}, \quad (6)$$

$$\tilde{c}_j = g_0 + g \times (j-1), \quad (7)$$

where c_0 is the number of initial input channels, g is a increasing factor of growth rate g_0 . C_i and \tilde{C}_i are the number of input channels in the i -th layer, c_j and \tilde{c}_j denote the output feature dimensionality of j -th convolutional layer.

From the above analysis, the group convolution is adopted to avoid the problem of parameter explosion. Note that we choose group convolution instead of conventional convolution since the former can reduce the number of parameters efficiently. Specifically, the corresponding parameters of them are given as

$$P_i = C_i^{out} \times C_i^{in} \times K \times K, \quad (8)$$

$$P_i^G = G_i \times \left(\frac{C_i^{out}}{G_i} \times \frac{C_i^{in}}{G_i} \times K \times K \right) = \frac{P_i}{G_i}, \quad (9)$$

where C_i^{in} and C_i^{out} are the number of input and output channels in the i -th layer, K indicates the corresponding kernel size, G_i is the group size and the bias is omitted for simplicity. Obviously, the parameters of group convolution (P_i^G) are less than the parameters of conventional convolution (P_i). However, when G_i is fixed, this will also cause the parameter to increase sharply since the output feature channels C_i^{out} grows up linearly with the dense layers. Therefore, we introduce the adaptive group convolution to further alleviate the parameter explosion. In the experiment, the group size is set to grow linearly with dense convolutional layers,

$$G_i = i + 1. \quad (10)$$

Moreover, the bottleneck architecture (1×1 convolutional filters) is also designed to refine the input cascaded features

to be consistent with the output channels of the corresponding layer, which can keep them divisible by the group size and boost the information propagation among different group features in each layer.

2) Joint Attention Mechanism (JA): The aim of the attention-based SR methods is to selectively focus on more important high-frequency details of the input feature for HR image recovery. Here, we introduce a novel joint attention that can capture cross-dimension dependencies [31] for improving the discriminative feature representations. First, we will revisit some attention mechanisms including channel attention and spatial attention [28, 29].

Convolutional Block Attention Module: Unlike SENet [28], convolutional block attention module (CBAM) [29] compute channel attention by using global average pooling and global max pooling. Specifically, let $X \in \mathbb{R}^{C \times H \times W}$ denote the input feature where C is the number of input channels, H and W are height and width of the input features, respectively. The channel-wise global statistics are defined as

$$GAP(X) = \frac{1}{H \times W} \sum_{i=1}^H \sum_{j=1}^W X_{i,j}, \quad (11)$$

$$GMP(X) = \max_{H,W} (X_{i,j}). \quad (12)$$

Next, the multi-layer perception is shared to compute channel attention,

$$A_e = \sigma(W_2 \delta(W_1 GAP(X)) + W_2 \delta(W_1 GMP(X))), \quad (13)$$

where σ and δ are the sigmoid function and the Rectified Linear Unit [32], $W_1 \in \mathbb{R}^{\frac{C}{r} \times C \times 1 \times 1}$, $W_2 \in \mathbb{R}^{C \times \frac{C}{r} \times 1 \times 1}$, and r is the reduction ratio. Moreover, the above average pooling and max pooling operations along the channel dimension are also used to produce the spatial attention weights in CBAM. The formulation can be written by

$$A_s = \sigma(w^{k \times k}([X_s^{avg}, X_s^{max}]])), \quad (14)$$

where $X_s^{avg}, X_s^{max} \in \mathbb{R}^{1 \times H \times W}$, $W^{k \times k}$ denotes a convolutional layer with the filter size of $k \times k$ and σ is the sigmoid function.

Joint Attention module: Although CBAM [29] introduces channel attention and spatial attention to improve the feature representations, they ignore the importance of cross-dimension interaction. For this problem, we propose the joint attention to effectively model channel attention and spatial attention with few parameters.

As shown in Fig. 2 (b), joint attention consists of four branches, two branches are responsible for modeling the channel attention ($C \times 1 \times 1$) and the spatial attention (H, W). The rest two branches aim to capture the interaction between the channel dimension and the spatial dimensions ((H, C) or (C, W)). Specifically, given a input feature map $X \in \mathbb{R}^{C \times H \times W}$. In the channel attention branch, like SENet [28], the channel attention weights are used to refine the feature \hat{X}_C . In the spatial attention branch, we first aggregate channel information to produce two 2D maps ($1 \times H \times W$) by the above average-pooling and max-pooling operations across the channel axis. Then, a 3×3 dilated convolution [33]

TABLE I
ABLATION STUDY OF DIFFERENT COMBINATIONS IN THE METHOD. WE REPORT THE PARAMETERS, FLOPs AND PSNR ON MANGA109 ($\times 4$).

	P_1	P_2	P_3	P_4
Channel attention [28]		✓		
Channel and Spatial attention [29]			✓	
Joint attention				✓
Params (K)	1471	1586	1588	1587
FLOPs (G)	31.78	31.85	31.87	31.87
PSNR (dB)	30.47	30.59	30.46	30.64

with dilation value 3 followed by a batch normalization [34] and a sigmoid activation function are used for producing the attention weights ($1 \times H \times W$). Finally, the spatial attention weights are multiplied with the input tensor X to generate the recalibrated feature $\hat{X}_{H \times W}$. For the remaining two branches, the input tensor X is first permuted and then passed to the above similar operations to generate the corresponding attention weights ($1 \times H \times C$ or $1 \times C \times W$), respectively. Subsequently, the generated attention weights are applied on the permuted feature and then rotated 90° clockwise along the width axis or the height axis to retain the original input shape ($C \times H \times W$). Finally, the refined features of four branches (\hat{X}_C , $\hat{X}_{H \times W}$, $\hat{X}_{H \times C}$, $\hat{X}_{C \times W}$) are aggregated by the averaging operation to enhance the discriminative representation ability of the network, which can be written as

$$\hat{X} = \frac{\hat{X}_C + \hat{X}_{H \times W} + \hat{X}_{H \times C} + \hat{X}_{C \times W}}{4}, \quad (15)$$

where \hat{X} is the output recalibrated feature. In addition to simple averaging, other simple and efficient aggregation methods can also be explored to further improve the performance.

III. EXPERIMENTAL RESULTS AND ANALYSIS

A. Datasets and Metrics

In our experiments, we use DIV2K dataset [35] as our training set, which contains 800 high-quality training images. We employ five standard benchmark datasets for testing our model, including Set5 [36], Set14 [37], Bsd100 [38], Urban100 [39] and Manga109 [40]. We conduct three different experiments with bicubic (BI), blur-downscale (BD) and downscale-noise (DN) degradation models. The peak signal-to-noise ratio (PSNR) and the structural similarity index measurement (SSIM) [41] are used for measuring the quality of the SR images on the luminance (Y) channel of the transformed YCbCr space.

B. Implementation Details

To construct the training pairs, we downsample the original HR images to generate LR Images by using bicubic interpolation. Data augmentation is performed on the above training dataset by randomly rotating 90° , 180° , 270° and flipping horizontally. In each training batch, 16 LR RGB patches with the size of 48×48 are randomly sampled as inputs. We adopt Adam optimizer [42] to train the model by setting $\beta_1 = 0.9$, $\beta_2 = 0.999$, and $\varepsilon = 10^{-8}$. The learning rate is initialized as 10^{-4} and reduced to half every 200 epochs. We implement

the proposed method by using the PyTorch framework [43] with a NVIDIA RTX 2080Ti GPU.

In our proposed model, the convolutional layers are set to 64 filters with 3×3 kernel size except for 1×1 convolutional layers for feature fusion. Additionally, in each pyramidal dense block, the initial input features are first reduced to c_0 and then passed to the subsequent pyramidal dense connection layers. For simplicity, the channel number of pyramidal dense layers can be expressed linearly as $c_j = (j + 1) \times c_0$. The operations of each pyramidal dense layer consists of a 1×1 convolution filter, activation function ReLU, 3×3 adaptive group convolution and ReLU. Specifically, c_0 is set to 16 and the number of pyramidal dense layers is 4 in a pyramidal dense block. Following the previous papers, we use the recently popular sampling method ESPCNN [17] to perform the upsampling operation. The final convolution layer has 3 filters with kernel size of 3×3 that are used to reconstruct the HR image.

C. Ablation Study

In this subsection, we analyze the effects of the key configurations in our proposed method. For fair comparisons, our method and its variants are set with the same baseline structure. As shown in Table I, we can see that the baseline method P_1 (without any attention) performs not very well and PSNR only reaches 30.47 dB on Manga109 ($\times 4$). It is noticed that when we compare the joint attention (P_4) with other attention mechanisms (P_2 and P_3), we can see that our joint attention module can achieve better performance (i.e., 30.64 v.s. 30.59 dB v.s. 30.46 dB).

In addition, we also compare other metrics, including parameters and FLOPs to demonstrate the effectiveness of our method. FLOPs is computed on the HR image with 512×512 pixels. From Table I, it is observed that our joint attention model can improve the PSNR with less additional parameters and FLOPs. The results clearly indicate that joint attention is more effective than other attention mechanisms [28, 29].

D. Results with Bicubic Degradation (BI)

We compare our proposed method with some state-of-the-art SR methods, Bicubic, SRCNN [4], FSRCNN [16], VDSR [44], DRCN [5], LapSRN [45], DRRN [6], SRMDNF [46], SRResNet [47] and CARN [19]. Table II shows quantitative results for three different scaling factors ($\times 2$, $\times 3$, $\times 4$). In addition, the number of parameters of these methods is also provided to show the model complexity. The results show

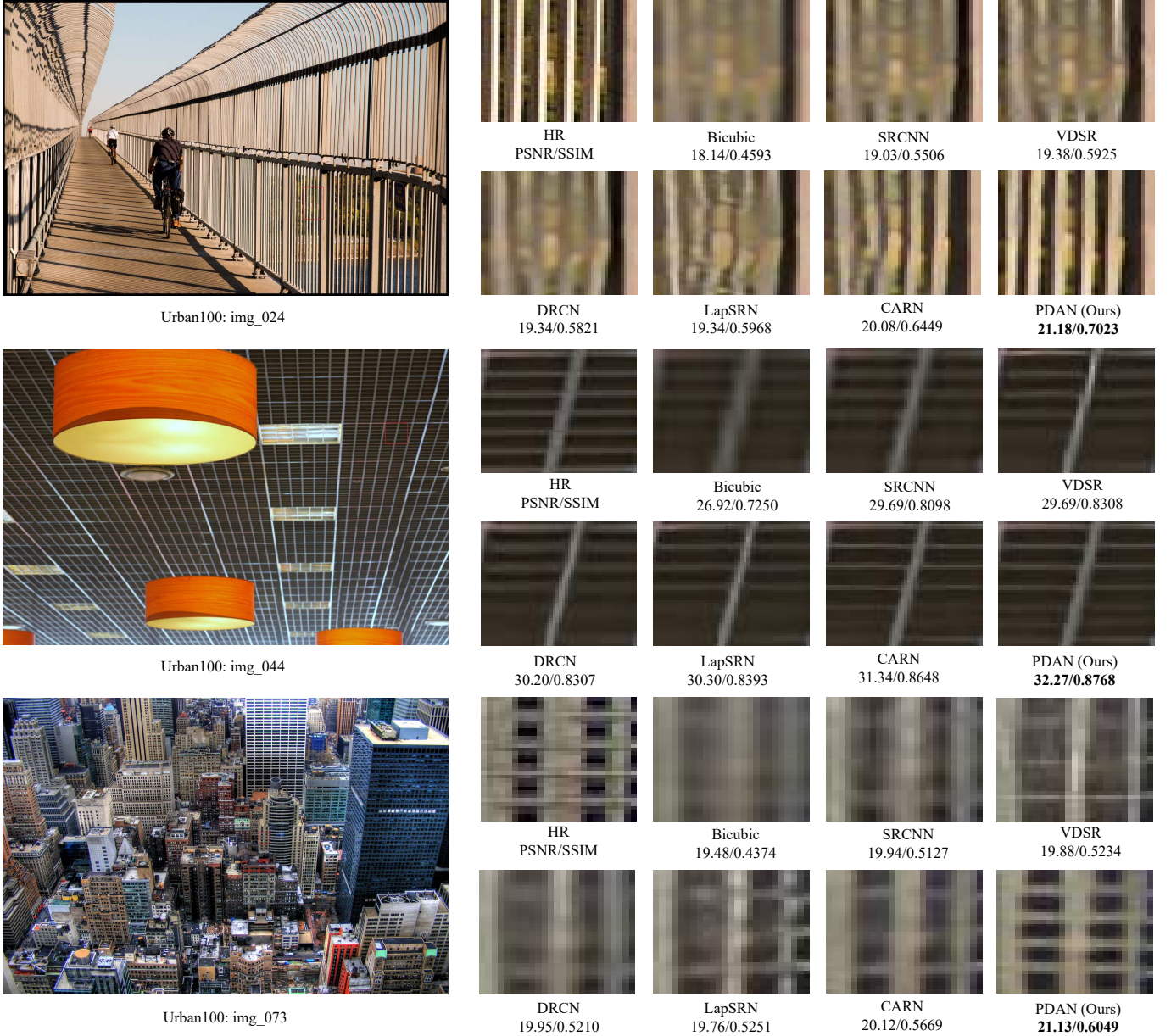


Fig. 3. Visual comparison for $\times 4$ SR with BI model on Urban100 dataset. The best results are highlighted.

that our PDAN achieves the comparable results on all the datasets and scaling factors in terms of both PSNR and SSIM. Although CARN [19] has similar parameters as us, our PDAN can obtain superior performance. For example, when the scaling factor is $\times 4$, the average PSNR gain of our PDAN over the CARN [19] are 0.20 dB, 0.17 dB on Urban100 and Manga109 datasets, respectively.

In Fig. 3, we present visual comparison with upscaling factor $\times 4$ on Urban100 dataset. We can see that our method yields best visual results among all existing compared methods. For “image_024”, the other compared methods generate the blurred detailed textures. Our method can recover more accurate lines and details. For “image_073”, most methods suffer from the blurry effects while our method produces the sharper edges and finer details.

E. Results with BD and DN Degradations

Following [14, 48], we also carry out experiments with blur-downscale (BD) and downscale-noise (DN) degradation models. The proposed method PDAN is compared with some state-of-the-art SR methods: SRCNN [4], FSRCNN [16], VDSR [44], IRCNN_G [48], IRCNN_C [48], SRMDNF [46], and RDN [14]. As shown in Table III, our PDAN achieves the best performance on almost all quantitative results compared with other SR methods with scaling factor $\times 3$. In particular, in comparison with RDN [14], our proposed PDAN still obtains comparable results. It is worth noting that PDAN has fewer parameters than RDN (1.6 M v.s. 22.3 M, $14\times$ less).

TABLE II
QUANTITATIVE RESULTS OF DIFFERENT IMAGE SR METHODS WITH BI DEGRADATION MODULE. THE PARAMETERS AND PSNR/SSIM COMPARISON RESULTS FOR SCALING FACTOR $\times 2$, $\times 3$ AND $\times 4$. RED/BLUE TEXT: BEST/SECOND-BEST AMONG ALL METHODS.

Methods	Scale	Params	Set5		Set14		Bsd100		Urban100		Manga109	
			PSNR	SSIM	PSNR	SSIM	PSNR	SSIM	PSNR	SSIM	PSNR	SSIM
Bicubic	2	—	33.66	0.9299	30.24	0.8688	29.56	0.8431	26.88	0.8403	30.80	0.9339
SRCNN [4]	2	57K	36.66	0.9542	32.45	0.9067	31.36	0.8879	29.50	0.8946	35.60	0.9663
FSRCNN [16]	2	13K	37.00	0.9558	32.63	0.9088	31.53	0.8920	29.88	0.9020	36.67	0.9710
VDSR [44]	2	666K	37.53	0.9587	33.03	0.9124	31.90	0.8960	30.76	0.9140	37.22	0.9750
DRCN [5]	2	1774K	37.63	0.9588	33.04	0.9118	31.85	0.8942	30.75	0.9133	37.55	0.9732
LapSRN [45]	2	251K	37.52	0.9591	32.99	0.9124	31.80	0.8952	30.41	0.9103	37.27	0.9740
DRRN [6]	2	298K	37.74	0.9591	33.23	0.9136	32.05	0.8973	31.23	0.9188	37.88	0.9749
SRMDNF [46]	2	1511K	37.79	0.9601	33.32	0.9159	32.05	0.8985	31.33	0.9204	38.07	0.9761
SRResNet [47]	2	1370K	38.05	0.9607	33.64	0.9178	32.22	0.9002	32.23	0.9295	38.05	0.9607
CARN [19]	2	1592K	37.76	0.9590	33.52	0.9166	32.09	0.8978	31.92	0.9256	38.36	0.9765
PDAN (ours)	2	1439K	38.05	0.9607	33.65	0.9182	32.20	0.8998	32.36	0.9300	38.71	0.9771
Bicubic	3	—	30.39	0.8682	27.55	0.7742	27.21	0.7385	24.46	0.7349	26.95	0.8556
SRCNN [4]	3	57K	32.75	0.9090	29.30	0.8215	28.41	0.7863	26.24	0.7989	30.48	0.9117
FSRCNN [16]	3	13K	33.18	0.9140	29.37	0.8240	28.53	0.7910	26.43	0.8080	31.10	0.9210
VDSR [44]	3	666K	33.66	0.9213	29.77	0.8314	28.82	0.7976	27.14	0.8279	32.01	0.9340
DRCN [5]	3	1774K	33.82	0.9226	29.76	0.8311	28.80	0.7963	27.15	0.8276	32.24	0.9343
LapSRN [45]	3	502K	33.81	0.9220	29.79	0.8325	28.82	0.7980	27.07	0.8275	32.21	0.9350
DRRN [6]	3	298K	34.03	0.9244	29.96	0.8349	28.95	0.8004	27.53	0.8378	32.71	0.9379
SRMDNF [46]	3	1528K	34.12	0.9254	30.04	0.8382	28.97	0.8025	27.57	0.8398	33.00	0.9403
SRResNet [47]	3	1554K	34.41	0.9274	30.36	0.8427	29.11	0.8055	28.20	0.8535	33.54	0.9448
CARN [19]	3	1592K	34.29	0.9255	30.29	0.8407	29.06	0.8034	28.06	0.8493	33.50	0.9440
PDAN (ours)	3	1624K	34.44	0.9276	30.39	0.8437	29.11	0.8063	28.34	0.8563	33.63	0.9448
Bicubic	4	—	28.42	0.8104	26.00	0.7027	25.96	0.6675	23.14	0.6577	24.89	0.7866
SRCNN [4]	4	57K	30.48	0.8628	27.50	0.7513	26.90	0.7101	24.52	0.7221	27.58	0.8555
FSRCNN [16]	4	12K	30.72	0.8660	27.61	0.7550	26.98	0.7150	24.62	0.7280	27.90	0.8610
VDSR [44]	4	665K	31.35	0.8830	28.02	0.7680	27.29	0.7251	25.18	0.7540	28.83	0.8870
DRCN [5]	4	1774K	31.53	0.8854	28.02	0.7670	27.23	0.7233	25.14	0.7510	28.98	0.8816
LapSRN [45]	4	813K	31.54	0.8850	28.19	0.7720	27.32	0.7270	25.21	0.7560	29.09	0.8900
DRRN [6]	4	297K	31.68	0.8888	28.21	0.7720	27.38	0.7284	25.44	0.7638	29.45	0.8946
SRMDNF [46]	4	1552K	31.96	0.8925	28.35	0.7787	27.49	0.7337	25.68	0.7731	30.09	0.9024
SRResNet [47]	4	1518K	32.17	0.8951	28.61	0.7823	27.59	0.7365	26.12	0.7871	30.48	0.9087
CARN [19]	4	1592K	32.13	0.8937	28.60	0.7806	27.58	0.7349	26.07	0.7837	30.47	0.9084
PDAN (ours)	4	1587K	32.28	0.8957	28.66	0.7831	27.62	0.7378	26.27	0.7922	30.64	0.9098

TABLE III
QUANTITATIVE RESULTS WITH BD AND DN DEGRADATION MODULES FOR SCALING FACTOR $\times 3$. RED/BLUE TEXT: BEST/SECOND-BEST AMONG ALL METHODS.

Methods	Model	Set5		Set14		Bsd100		Urban100		Manga109	
		PSNR	SSIM	PSNR	SSIM	PSNR	SSIM	PSNR	SSIM	PSNR	SSIM
Bicubic	BD	28.78	0.8308	26.38	0.7271	26.33	0.6918	23.52	0.6862	25.46	0.8149
	DN	24.01	0.5369	22.87	0.4724	22.92	0.4449	21.63	0.4687	23.01	0.5381
SRCNN [4]	BD	32.05	0.8944	28.80	0.8074	28.13	0.7736	25.70	0.7770	29.47	0.8924
	DN	25.01	0.6950	23.78	0.5898	23.76	0.5538	21.90	0.5737	23.75	0.7148
FSRCNN [16]	BD	26.23	0.8124	24.44	0.7106	24.86	0.6832	22.04	0.6745	23.04	0.7927
	DN	24.18	0.6932	23.02	0.5856	23.41	0.5556	21.15	0.5682	22.39	0.7111
VDSR [44]	BD	33.25	0.9150	29.46	0.8244	28.57	0.7893	26.61	0.8136	31.06	0.9234
	DN	25.20	0.7183	24.00	0.6112	24.00	0.5749	22.22	0.6096	24.20	0.7525
IRCNN_G [48]	BD	33.38	0.9182	29.63	0.8281	28.65	0.7922	26.77	0.8154	31.15	0.9245
	DN	25.70	0.7379	24.45	0.6305	24.28	0.5900	22.90	0.6429	24.88	0.7765
IRCNN_C [48]	BD	33.17	0.9157	29.55	0.8271	28.49	0.7886	26.47	0.8081	31.13	0.9236
	DN	27.48	0.7925	25.92	0.6932	25.55	0.6481	23.93	0.6950	26.07	0.8253
SRMDNF [46]	BD	34.09	0.9242	30.11	0.8364	28.98	0.8009	27.50	0.8370	32.97	0.9391
	DN	27.74	0.8026	26.13	0.6974	25.64	0.6495	24.28	0.7092	26.72	0.8424
PDAN (ours)	BD	34.47	0.9270	30.43	0.8425	29.16	0.8058	28.28	0.8533	33.85	0.9448
	DN	28.51	0.8156	26.57	0.7101	25.93	0.6600	24.84	0.7340	27.88	0.8574
RDN [14]	BD	34.58	0.9280	30.53	0.8447	29.23	0.8079	28.46	0.8582	33.97	0.9465
	DN	28.47	0.8151	26.60	0.7101	25.93	0.6573	24.92	0.7364	28.00	0.8591

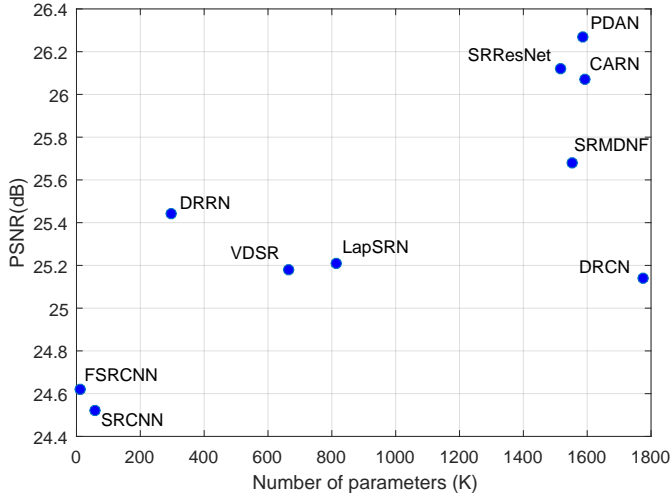


Fig. 4. PSNR v.s. Parameters. The PSNR values are evaluated on Urban100 with scaling factor $\times 4$

F. Model size

The number of parameters is a key factor for constructing a lightweight image SR model. From Table II, we can observe that our method achieve better results than other state-of-the-art lightweight methods. As shown in Fig. 4, we illustrate the comparisons about parameters and PSNR on Urban100 with upscaling factor $\times 4$. In comparison with other methods, our PDAN obtains superior performance with comparable model size. It demonstrates that our method achieves a better trade-off between the performance and model size.

IV. CONCLUSION

In this paper, we propose a lightweight pyramidal dense attention network (PDAN) for image SR. Specifically, in the proposed pyramidal dense attention block, the pyramidal dense connections can efficiently exploit feature information in different layers. Meanwhile, the adaptive group convolution whose group size increases linearly with layers is presented to relieve the parameter explosion. In addition, we introduce a new joint attention mechanism to recalibrate the feature responses more accurately by considering cross-dimension interaction in an efficient way. Extensive experiments on image SR demonstrate the superior performance of our PDAN in terms of quantitative and qualitative results.

REFERENCES

- [1] F. Zhou, W. Yang, and Q. Liao, "Interpolation-based image super-resolution using multisurface fitting," *IEEE Transactions on Image Processing*, vol. 21, no. 7, pp. 3312–3318, 2012.
- [2] Y. W. Tai, S. Liu, M. S. Brown, and S. Lin, "Super resolution using edge prior and single image detail synthesis," in *Proceedings of the IEEE Conference on Computer Vision and Pattern Recognition*, 2010.
- [3] R. Timofte, V. De Smet, and L. Van Gool, "A+: Adjusted anchored neighborhood regression for fast super-resolution," in *Asian Conference on Computer Cision*. Springer, 2014, pp. 111–126.

- [4] C. Dong, C. C. Loy, K. He, and X. Tang, "Image super-resolution using deep convolutional networks," *IEEE Transactions on Pattern Analysis and Machine Intelligence*, vol. 38, no. 2, pp. 295–307, 2015.
- [5] J. Kim, J. Kwon Lee, and K. Mu Lee, "Deeply-recursive convolutional network for image super-resolution," in *Proceedings of the IEEE Conference on Computer Vision and Pattern Recognition*, 2016, pp. 1637–1645.
- [6] Y. Tai, J. Yang, and X. Liu, "Image super-resolution via deep recursive residual network," in *Proceedings of the IEEE Conference on Computer Vision and Pattern Recognition*, 2017.
- [7] Y. Tang, W. Gong, X. Chen, and W. Li, "Deep inception-residual laplacian pyramid networks for accurate single image super-resolution," *IEEE Transactions on Neural Networks and Learning Systems*, vol. 31, no. 5, 2017.
- [8] B. Lim, S. Son, H. Kim, S. Nah, and K. Mu Lee, "Enhanced deep residual networks for single image super-resolution," in *Proceedings of the IEEE Conference on Computer Vision and Pattern Recognition Workshops*, 2017, pp. 136–144.
- [9] J. Xin, J. Li, X. Jiang, N. Wang, H. Huang, and X. Gao, "Wavelet-based dual recursive network for image super-resolution," *IEEE Transactions on Neural Networks and Learning Systems*, vol. PP, no. 99, pp. 1–14, 2020.
- [10] H. Wu, Z. Zou, J. Gui, W. Zeng, J. Ye, J. Zhang, H. Liu, and Z. Wei, "Multi-grained attention networks for single image super-resolution," *IEEE Transactions on Circuits and Systems for Video Technology*, vol. PP, no. 99, pp. 1–1, 2020.
- [11] Z. Wang, J. Chen, and S. C. H. Hoi, "Deep learning for image super-resolution: A survey," *IEEE Transactions on Pattern Analysis and Machine Intelligence*, vol. PP, no. 99, pp. 1–1, 2020.
- [12] K. He, X. Zhang, S. Ren, and J. Sun, "Deep residual learning for image recognition," in *Proceedings of the IEEE Conference on Computer Vision and Pattern Recognition*, 2016, pp. 770–778.
- [13] G. Huang, Z. Liu, L. Van Der Maaten, and K. Q. Weinberger, "Densely connected convolutional networks," in *Proceedings of the IEEE Conference on Computer Vision and Pattern Recognition*, 2017, pp. 4700–4708.
- [14] Y. Zhang, Y. Tian, Y. Kong, B. Zhong, and Y. Fu, "Residual dense network for image super-resolution," in *Proceedings of the IEEE Conference on Computer Vision and Pattern Recognition*, 2018, pp. 2472–2481.
- [15] T. Dai, J. Cai, Y. Zhang, S. Xia, and L. Zhang, "Second-order attention network for single image super-resolution," in *Proceedings of the IEEE Conference on Computer Vision and Pattern Recognition*, 2019, pp. 11 065–11 074.
- [16] C. Dong, C. C. Loy, and X. Tang, "Accelerating the super-resolution convolutional neural network," in *Proceedings of the European Conference on Computer Vision*. Springer, 2016, pp. 391–407.
- [17] W. Shi, J. Caballero, F. Huszár, J. Totz, A. P. Aitken, R. Bishop, D. Rueckert, and Z. Wang, "Real-time single image and video super-resolution using an efficient sub-

- pixel convolutional neural network,” in *Proceedings of the IEEE Conference on Computer Vision and Pattern Recognition*, 2016, pp. 1874–1883.
- [18] Y. Zhang, K. Li, K. Li, L. Wang, B. Zhong, and Y. Fu, “Image super-resolution using very deep residual channel attention networks,” in *Proceedings of the European Conference on Computer Vision*, 2018, pp. 286–301.
- [19] N. Ahn, B. Kang, and K. A. Sohn, “Fast, accurate, and lightweight super-resolution with cascading residual network,” in *Proceedings of the European Conference on Computer Vision*, 2018.
- [20] T. Zhang, G. J. Qi, B. Xiao, and J. Wang, “Interleaved group convolutions for deep neural networks,” 2017.
- [21] Z. Hui, X. Wang, and X. Gao, “Fast and accurate single image super-resolution via information distillation network,” in *Proceedings of the IEEE Conference on Computer Vision and Pattern Recognition*, 2018.
- [22] Z. Hui, X. Gao, Y. Yang, and X. Wang, “Lightweight image super-resolution with information multi-distillation network,” in *Acm International Conference*, 2019.
- [23] K. Zhang, S. Gu, R. Timofte, Z. Hui, X. Wang, X. Gao, D. Xiong, S. Liu, R. Gang, N. Nan, C. Li, X. Zou, N. Kang, Z. Wang, H. Xu, C. Wang, Z. Li, L. Wang, J. Shi, W. Sun, Z. Lang, J. Nie, W. Wei, L. Zhang, Y. Niu, P. Zhuo, X. Kong, L. Sun, and W. Wang, “Aim 2019 challenge on constrained super-resolution: Methods and results,” in *2019 IEEE/CVF International Conference on Computer Vision Workshops*, 2019, pp. 3565–3574.
- [24] A. G. Howard, M. Zhu, B. Chen, D. Kalenichenko, W. Wang, T. Weyand, M. Andreetto, and H. Adam, “Mobilenets: Efficient convolutional neural networks for mobile vision applications,” 2017.
- [25] J. J. Liu, Q. Hou, M. M. Cheng, C. Wang, and J. Feng, “Improving convolutional networks with self-calibrated convolutions,” in *2020 IEEE/CVF Conference on Computer Vision and Pattern Recognition (CVPR)*, 2020.
- [26] X. Chu, B. Zhang, H. Ma, R. Xu, J. Li, and Q. Li, “Fast, accurate and lightweight super-resolution with neural architecture search,” 2019.
- [27] Y. Hu, J. Li, Y. Huang, and X. Gao, “Channel-wise and spatial feature modulation network for single image super-resolution,” *IEEE Transactions on Circuits and Systems for Video Technology*, 2019.
- [28] J. Hu, L. Shen, and G. Sun, “Squeeze-and-excitation networks,” in *Proceedings of the IEEE Conference on Computer Vision and Pattern Recognition*, 2018, pp. 7132–7141.
- [29] S. Woo, J. Park, J. Y. Lee, and I. S. Kweon, “Cbam: Convolutional block attention module,” in *Proceedings of the European Conference on Computer Vision*, 2018.
- [30] Z. Zhu, Z. P. Bian, J. Hou, Y. Wang, and L. P. Chau, “When residual learning meets dense aggregation: Re-thinking the aggregation of deep neural networks,” 2020.
- [31] D. Misra, T. Nalamada, A. U. Arasanipalai, and Q. Hou, “Rotate to attend: Convolutional triplet attention module,” in *Proceedings of the IEEE/CVF Winter Conference on Applications of Computer Vision (WACV)*, January 2021, pp. 3139–3148.
- [32] X. Glorot, A. Bordes, and Y. Bengio, “Deep sparse rectifier neural networks,” in *Proceedings of the 14th International Conference on Artificial Intelligence and Statistics (AISTATS)*, 2011, pp. 315–323.
- [33] F. Yu and V. Koltun, “Multi-scale context aggregation by dilated convolutions,” 2016.
- [34] S. Ioffe and C. Szegedy, “Batch normalization: Accelerating deep network training by reducing internal covariate shift,” 2015.
- [35] R. Timofte, E. Agustsson, L. Van Gool, M.-H. Yang, and L. Zhang, “Ntire 2017 challenge on single image super-resolution: Methods and results,” in *Proceedings of the IEEE Conference on Computer Vision and Pattern Recognition Workshops*, 2017, pp. 114–125.
- [36] M. Bevilacqua, A. Roumy, C. Guillemot, and M. L. Alberi-Morel, “Low-complexity single-image super-resolution based on nonnegative neighbor embedding,” in *Proceedings of the British Machine Vision Conference*, 2012.
- [37] R. Zeyde, M. Elad, and M. Protter, “On single image scale-up using sparse-representations,” in *International Conference on Curves and Surfaces*. Springer, 2010, pp. 711–730.
- [38] D. Martin, C. Fowlkes, D. Tal, and J. Malik, “A database of human segmented natural images and its application to evaluating segmentation algorithms and measuring ecological statistics,” in *IEEE International Conference on Computer Vision*, 2002.
- [39] J.-B. Huang, A. Singh, and N. Ahuja, “Single image super-resolution from transformed self-exemplars,” in *Proceedings of the IEEE Conference on Computer Vision and Pattern Recognition*, 2015, pp. 5197–5206.
- [40] Y. Matsui, K. Ito, Y. Aramaki, A. Fujimoto, T. Ogawa, T. Yamasaki, and K. Aizawa, “Sketch-based manga retrieval using manga109 dataset,” *Multimedia Tools and Applications*, vol. 76, no. 20, pp. 21 811–21 838, 2017.
- [41] Z. Wang, A. C. Bovik, H. R. Sheikh, E. P. Simoncelli *et al.*, “Image quality assessment: from error visibility to structural similarity,” *IEEE Transactions on Image Processing*, vol. 13, no. 4, pp. 600–612, 2004.
- [42] D. Kingma and J. Ba, “Adam: A method for stochastic optimization,” *Computer Science*, 2014.
- [43] A. Paszke, S. Gross, S. Chintala, G. Chanan, E. Yang, Z. DeVito, Z. Lin, A. Desmaison, L. Antiga, and A. Lerer, “Automatic differentiation in pytorch,” 2017.
- [44] J. Kim, J. Kwon Lee, and K. Mu Lee, “Accurate image super-resolution using very deep convolutional networks,” in *Proceedings of the IEEE Conference on Computer Vision and Pattern Recognition*, 2016, pp. 1646–1654.
- [45] W.-S. Lai, J.-B. Huang, N. Ahuja, and M.-H. Yang, “Deep laplacian pyramid networks for fast and accurate super-resolution,” in *Proceedings of the IEEE Conference on Computer Vision and Pattern Recognition*, 2017, pp. 624–632.
- [46] K. Zhang, W. Zuo, and L. Zhang, “Learning a single convolutional super-resolution network for multiple degradations,” in *Proceedings of the IEEE Conference*

on *Computer Vision and Pattern Recognition*, 2018, pp. 3262–3271.

- [47] C. Ledig, L. Theis, F. Huszár, J. Caballero, A. Cunningham, A. Acosta, A. Aitken, A. Tejani, J. Totz, Z. Wang *et al.*, “Photo-realistic single image super-resolution using a generative adversarial network,” in *Proceedings of the IEEE Conference on Computer Vision and Pattern Recognition*, 2017, pp. 4681–4690.
- [48] K. Zhang, W. Zuo, S. Gu, and L. Zhang, “Learning deep cnn denoiser prior for image restoration,” in *Proceedings of the IEEE Conference on Computer Vision and Pattern Recognition*, 2017, pp. 3929–3938.